Influence of Subfacet Heterogeneity and Material Properties on the Urban Surface Energy Budget

PRATHAP RAMAMURTHY,* ELIE BOU-ZEID,* JAMES A. SMITH,* ZHIHUA WANG,+ MARY L. BAECK,* NICANOR Z. SALIENDRA,#,@ JOHN L. HOM,& AND CLAIRE WELTY#,**

* *Department of Civil and Environmental Engineering, Princeton University, Princeton, New Jersey*
+ *School of Sustainable Engineering and the Built Environment, Arizona State University, Tempe, Arizona*
# *Center for Urban Environmental Research and Education, University of Maryland Baltimore County, Baltimore, Maryland*
& *U.S. Department of Agriculture Forest Service, Newtown Square, Pennsylvania*
** *Department of Chemical, Biochemical and Environmental Engineering, University of Maryland Baltimore County, Baltimore, Maryland*

(Manuscript received 11 September 2013, in final form 17 January 2014)

ABSTRACT

Urban facets—the walls, roofs, and ground in built-up terrain—are often conceptualized as homogeneous surfaces, despite the obvious variability in the composition and material properties of the urban fabric at the subfacet scale. This study focuses on understanding the influence of this subfacet heterogeneity, and the associated influence of different material properties, on the urban surface energy budget. The Princeton Urban Canopy Model, which was developed with the ability to capture subfacet variability, is evaluated at sites of various building densities and then applied to simulate the energy exchanges of each subfacet with the atmosphere over a densely built site. The analyses show that, although all impervious built surfaces convert most of the incoming energy into sensible heat rather than latent heat, sensible heat fluxes from asphalt pavements and dark rooftops are 2 times as high as those from concrete surfaces and light-colored roofs. Another important characteristic of urban areas—the shift in the peak time of sensible heat flux in comparison with rural areas—is here shown to be mainly linked to concrete's high heat storage capacity as well as to radiative trapping in the urban canyon. The results also illustrate that the vegetated pervious soil surfaces that dot the urban landscape play a dual role: during wet periods they redistribute much of the available energy into evaporative fluxes but when moisture stressed they behave more like an impervious surface. This role reversal, along with the direct evaporation of water stored over impervious surfaces, significantly reduces the overall Bowen ratio of the urban site after rain events.

1. Introduction

Despite the complex geometry and the multitude of surfaces with varying hygrothermal and aerodynamic properties in urban terrain (Oke 1978), researchers have traditionally relied on the eddy covariance (EC) technique, which can only measure area-averaged sensible and latent heat fluxes, to characterize land–atmosphere interactions over such terrain (Roth 2007; Velasco et al. 2011; Grimmond et al. 2004; Rotach et al. 2005; Song and Wang 2012; Christen and Vogt 2004). Investigations of fluxes from individual facets or canyons exist (Nunez and Oke 1977, 1980; Nottrott et al. 2011) but are relatively rare. The general consensus from these studies is that urbanization significantly alters the Bowen ratio (Bo, the ratio of sensible to latent heat fluxes) by decreasing the latent heat flux (as a result of reduced surface moisture availability) and consequently increasing the sensible heat released into the atmosphere (Oke 1988; Grimmond and Oke 2002; Coutts et al. 2007; Ching 1985). In urbanized areas, the natural vegetative cover is replaced by practically impervious built surfaces such as concrete and asphalt that overwhelmingly convert the available energy into sensible heat. Even pervious land covers in urban terrain (parks, lawns, etc.) are likely to be engineered and built with different soil and vegetation

@ Current affiliation: U.S. Department of Agriculture Forest Service, Logan, Utah.

Corresponding author address: Elie Bou-Zeid, E414 EQUAD, Dept. of Civil and Environmental Engineering, Princeton University, Princeton, NJ 08544.
E-mail: ebouzeid@princeton.edu

DOI: 10.1175/JAMC-D-13-0286.1

FIG. 1. Land-cover characteristics surrounding all four flux towers (yellow triangles): (top left) the suburban Cub Hill site in Baltimore County, Maryland (39.4125°N, 76.5208°W), (top right) the UMBC tower (39.2542°N, 76.7097°W), (bottom left) the Broadmead site in Princeton (40.3464°N, 74.6435°W), and (bottom right) the tower over the built-up Princeton town/campus (40.3509°N, 74.6510°W). The images are copyright Google Earth.

properties than their natural counterparts; they are hence not necessarily ''natural.'' Therefore, to distinguish the urban land-cover types in this study, we will refer to impervious surfaces (concrete, asphalt, roofs, stone, etc.) and pervious surfaces (natural or engineered soils, grass, or other vegetated surfaces).

As an illustration of the impact of urbanization on the surface fluxes, Fig. 1 shows an aerial view of two pairs of adjacent sites and Fig. 2 compares the surface energy fluxes from these two pairs: Princeton–Broadmead is the first pair, located in Princeton, New Jersey, and University of Maryland, Baltimore County (UMBC)–Cub Hill is the second, located in Baltimore County, Maryland (site characterization and experimental details are provided later in the paper when the data are used for model validation). One site in each pair (Princeton and UMBC) is in a relatively densely built urban neighborhood, and the other site in the pair is located in a suburban area surrounded mainly by mature vegetation and mixed trees with some houses (Cub Hill) or grass (Broadmead). Note that the land cover surrounding the sites differs but both sites of a given pair are influenced by the same synoptic forcings. Figure 2 clearly reveals a shift in Bo in going from the built-up urban sites to the more vegetated suburban sites. At the suburban sites, the latent heat flux dominates because of the significant fraction of pervious surfaces. This dissimilarity between urban and suburban sites has been widely reported in the literature (e.g., Christen 2005; Grimmond and Oke 1999). Another important observation in these figures is that the available energy [the sum of the sensible heat flux H and latent heat flux LE into the atmosphere ($=R_n - Q$, where R_n is the net radiation and Q is the heat flux into the surface; we ignore anthropogenic emissions here for simplicity of illustration)] is much higher at the suburban site than at the urban site. Moreover, the diurnal trends of H show a maximum over the suburban site earlier in the day, whereas the peaks at the urban sites occur later. This phase shift has been observed previously and attributed to the higher thermal storage capacity of impervious surfaces (Ching 1985; Grimmond and Oke 1999; Offerle et al. 2005, 2006), but its dynamics have not been investigated in detail.

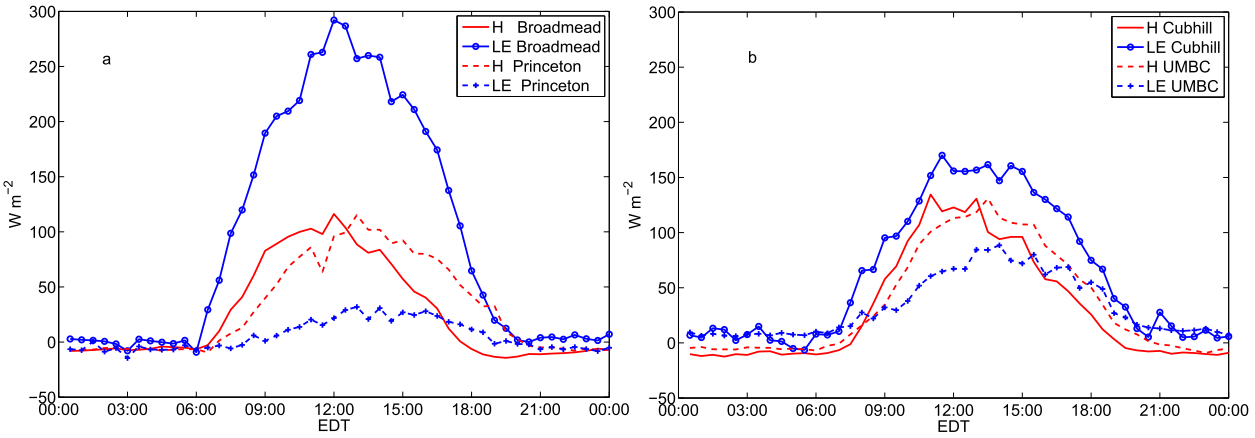

FIG. 2. Monthly-averaged diurnal cycles of sensible and latent heat fluxes, with 30-min resolution, for July 2009 from (a) the suburban Broadmead and densely built Princeton sites and (b) the suburban Cub Hill and densely built UMBC sites. EDT is UTC − 4 h.

These observations at the two pairs of sites that we study illustrate the well-known bulk influences of urbanization on the surface energy fluxes. Although these flux studies have contributed significantly to our understanding and have improved our ability to parameterize urban fluxes, they inherently lump the contributions from the various urban facets and materials and thus lack the capability to discern the effect of specific surfaces and hygrothermal properties associated with building-scale variability on the urban surface energy budget (SEB) (footprint analysis can allow them to capture neighborhood-scale variability). Such detailed, material-specific knowledge, however, is needed to develop better strategies for mitigation of the urban heat island (UHI) effect and other adverse environmental processes in cities and to guide urban design, including material selection for construction. Given the above-mentioned challenges in measuring facet and subfacet-scale fluxes, models of the urban surface energy budget are needed to develop this understanding.

Many researchers have relied on urban canopy models (UCMs) or the closely related coupled urban energy and water exchange schemes (Grimmond and Oke 2002; Kusaka et al. 2001; Masson 2000; Martilli et al. 2002; Järvi et al. 2011; Berthier et al. 2006; Hamdi and Schayes 2008) to study energy exchanges in urban areas. These models are primarily used to parameterize land–atmosphere interactions over urban areas in mesoscale models (Kusaka and Kimura 2004), but they have also been successfully used in offline mode to understand urban energy and water budgets (Wang et al. 2011a; Järvi et al. 2011). In addition, urban models have also been used to study UHI effects (Hamdi and Schayes 2008; Bohnenstengel et al. 2011).

In the last decade, UCMs have evolved from simple slab models to multilayer schemes that can account for various complex and interacting urban processes. Most UCMs now have the ability to distinguish among various urban facets like rooftops, roads, and walls. Moreover, the energy exchanges between various urban facets and the atmosphere are relatively well represented (although this aspect of UCMs can certainly still be significantly improved). Porson et al. (2009) studied the performance of different UCMs (from single-facet slab models to multifacet UCMs) and found that UCMs having two or more urban facets performed better than the slab models. Kusaka et al. (2012) also confirmed the superiority of UCMs over slab models in their study on the UHI over Tokyo. These developments have considerably improved the ability of UCMs to model urban radiative exchanges (Grimmond et al. 2010, 2011), but most UCMs continue to have a very simplistic representation of urban subfacets and to lump the hygrothermal properties and dynamics of different subfacets into an "average urban facet," which is often difficult to define or characterize. Because of these limitations, as well as the simplistic treatment of urban hydrological behavior and pervious surfaces, UCMs perform poorly in modeling turbulent exchanges—in particular, latent heat fluxes (Grimmond et al. 2010, 2011).

To address these limitations, the Princeton UCM (PUCM) has been developed with distinct representation for various subfacets and a more realistic and complete inclusion of hydrological processes. Rooftops in PUCM can be represented as any combination of black, white, and green roofs, each modeled independently using its unique physical and thermal attributes. Likewise, the ground facet can be segregated into asphalt, concrete, and grass fractions (more facets such as brick pavements can be added). Apart from these additions, PUCM is further enhanced in two key aspects: 1) a detailed hydrological model, which uses the Richards equation to

TABLE 1. Meteorological data used to force PUCM at the UMBC and Cub Hill sites.

	UMBC	Cub Hill
Incoming longwave (LW) and shortwave (SW) radiation	No radiometer; incoming SW and LW radiation measured at Cub Hill were used	Kipp & Zonen CNR1, which includes the CM3 thermopile pyranometer and the CG3 pyrgeometer
Air temperature	Vaisala, Inc., HMP45	R.M. Young Co. T/RH 500
Specific humidity	Vaisala HMP45	R.M. Young T/RH 500
Wind speed	Campbell Scientific, Inc., CSAT3	R.M. Young IU1
Atmospheric pressure	Li-Cor, Inc., 7500	Vaisala PTB101B
Precipitation	All Weather, Inc., rain gauge 6011-A	Weathertronics International, Inc., rain gauge 6011-B

simulate vertical water transport in urban pervious surfaces while assigning a nonzero water-holding capacity for impervious surfaces, is included to predict urban water storage and evaporative fluxes (Wang et al. 2013) and 2) conduction in solids is modeled using more accurate spatially analytical solutions (as compared with the more common finite-difference numerical solutions) of the one-dimensional heat equation (Wang et al. 2013). These additions, along with calibration of some urban material properties specifically for the northeastern United States (Wang et al. 2011a), where validation was conducted, have significantly improved PUCM's ability to model H and LE (Wang et al. 2011b, 2013).

In this study, we particularly exploit PUCM's ability to model subfacet fluxes with the aim of studying their variability, their sensitivity to material properties, and their influence on the integrated urban surface energy budget. The model is first briefly presented and evaluated using observed data from all four sites discussed above. In these validations, PUCM is run with the characteristic urban properties determined over the EC measurement footprint (which can vary with wind direction). The meteorological data observed at the various towers are used to force (provide the state of the atmosphere for) the model. The UMBC site is subsequently selected (because of unique characteristics that we detail later) for further modeling and analysis aimed at answering the overarching questions of this study: 1) How does the variability in surface hygrothermal properties translate into variability in surface–atmosphere fluxes at the subfacet and urban scales? 2) How is this variability influenced by hydrometeorological conditions?

2. Model methods, setup, and evaluation

a. Methods

PUCM combines basic meteorological data with aerodynamic and geometric properties of the built environment and hygrothermal properties of impervious and pervious surfaces to estimate the surface energy budget for urban canopies [see Wang et al. (2013) for an in-depth model description and validation]. The model is based on the urban energy exchange schemes devised by Masson (2000) and Kusaka et al. (2001). It is a single-layer UCM, but with the unique ability to represent multiple surfaces and materials in each of the UCM facets (ground, wall, and roof). PUCM also includes a detailed hydrologic component to account for bare-soil evaporation and evaporation from impervious surfaces (asphalt and concrete ground pavements, roofs, etc.). Impervious surfaces are modeled to have variable water holding/storage, capped by a fixed upper limit like a bucket model (see Table 3, described in more detail below, for maximum allowed water capacity for various surfaces). The storage is replenished by precipitation and then depleted by evaporation at a rate that is reduced from the potential evaporation by a factor β_I (=actual storage/maximum storage). For pervious surfaces, the Richards equation is solved numerically over multiple layers to describe water storage and transport and surface evapotranspiration is reduced from the potential rate as the surface soil moisture is reduced below saturation and as a result of the stomatal resistance of the vegetation. The aerodynamic transfer functions (aerodynamic resistances that control the fluxes from each subfacet) are stability dependent and different for different facets, but the same functions are used for the different subfacets within each facet. The model is forced by basic meteorological variables measured at the flux sites as detailed in Tables 1 and 2. Note that the model can account for anthropogenic heat fluxes by adding them as sources wherever they occur (e.g., car heat emissions can be added inside the canyon); however, because the model is not applied over very dense urban cores (such as downtowns or industrial neighborhoods) in this study, the contribution from this term is neglected. This term would not be large enough to have a significant impact on our results and its value would have high uncertainty.

b. Model setup

In addition to forcing data, site characteristics need to be specified to run PUCM. The footprint for each flux tower was calculated, and the surface characteristics in PUCM were set to match the footprint characteristics. Given the uncertainty in determining the footprint over

TABLE 2. Meteorological data used to force PUCM at the Princeton and Broadmead sites.

	Princeton	Broadmead
Incoming LW and SW radiation	Hukseflux Thermal Sensors B.V. four-component net radiation sensor NR01	Hukseflux four-component net radiation sensor NR01
Air temperature	Vaisala HMP45C	Vaisala HMP45C
Specific humidity	Vaisala HMP45C	Vaisala HMP45C
Wind speed	Campbell Scientific CSAT3	Campbell Scientific CSAT3
Atmospheric pressure	Li-Cor 7500	Li-Cor 7500
Precipitation	No precipitation gauge; precipitation measured at Broadmead was used	CS700 tipping-bucket rain gauge

heterogeneous surfaces and the difficulty in properly characterizing the surface properties, the comparison between model output and field observations is used only to confirm the agreement of the qualitative trends; exact quantitative agreement is not expected. Hence this part of the study should be viewed as a model-evaluation analysis. PUCM has been quantitatively validated using sensor networks (Wang et al. 2013); in those validations, model surface temperatures for different subfacets and materials agreed very well with observed temperatures. In addition, the model was shown to accurately capture soil moisture increase due to precipitation and the subsequent decrease during dry down. In this study, we test the model's ability to qualitatively reproduce the SEB differences among the sites with different surface materials and composition so that we can then use it to probe the surface physical mechanisms and properties that induce the dissimilarity in surface fluxes between urban and rural sites, as well as to study the influence of material properties on the urban SEB.

Particular attention is paid to the UMBC site, the focus of our modeling efforts. For the UMBC simulations, the land surface is divided into four sectors, each with distinct land-cover characteristics. This is needed because of the strong variability of upwind surface properties at the site, depending on wind direction. The model is run separately for each sector, and the results, only when compared with observed data, are then aggregated using observed wind direction measurements (at any given time, the fluxes from the upwind sector are used). This sectoring is depicted in Fig. 3, and the land-cover partitioning for each sector is detailed in the pie chart in Fig. 4. This aggregation is only needed in the model-evaluation part since the model footprint needs to match the EC footprint. In subsequent analyses when no comparison with observed data is performed, the fluxes from all sectors are averaged with equal weights to represent the integrated true SEB of the site.

The tower footprints were estimated using the analytical model proposed by Hsieh et al. (2000). Although the footprint was estimated by assuming neutral conditions (a dynamic determination for each 30-min period would make modeling very complicated, because it would entail redefining the surface properties for each period), PUCM does account for stability when computing the aerodynamic transfer functions of each facet. Figure 3 shows the computed footprint used to configure PUCM for the UMBC site. Lawns and parking lots cover most of sector II, and sector III has a high concentration of buildings. Sectors IV and I have an even distribution of impervious and pervious (mostly grass) surfaces. PUCM does not yet have the ability to represent the tall trees that cover a small fraction in sectors II and III; therefore, tree cover is represented as a grass surface in this study. The average height of the buildings around the tower is approximately 9 m, and the flux tower is 24.5 m AGL. Depending on the wind direction, a few individual buildings can affect the flux measurements because the EC sensors occasionally lie in the roughness sublayer; raising the EC level significantly above all surrounding buildings would make the footprint almost completely outside the UMBC campus, however, and thus would lead to other biases. The EC data for all sites were treated in the standard way (Foken et al. 2005) to compute fluxes: the planar-fit and Webb–Pearman–Leuning corrections were applied, the corrected fields were linearly detrended, and the instantaneous fluxes were averaged over a period of 30 min.

Crawford et al. (2011) did an extensive land-cover analysis of the Cub Hill site, which we use to represent the surface in our simulations. Overall, 68% of the area at that site is covered by vegetation and the rest is split among rooftops, asphalt, and concrete pavements. The suburban Broadmead site is overwhelmingly surrounded by grass, 10–15 cm tall. The footprint at the Princeton site and its urban characteristics are obtained from Wang et al. (2013). In addition to the forcings and land-cover characteristics described above, the thermal, aerodynamic, and soil properties are prescribed in the model as shown in Table 3.

c. *Model evaluation*

From the setup detailed in section 2b, PUCM model simulations were run for the months of July 2009 at the UMBC and Cub Hill sites and July 2011 for the

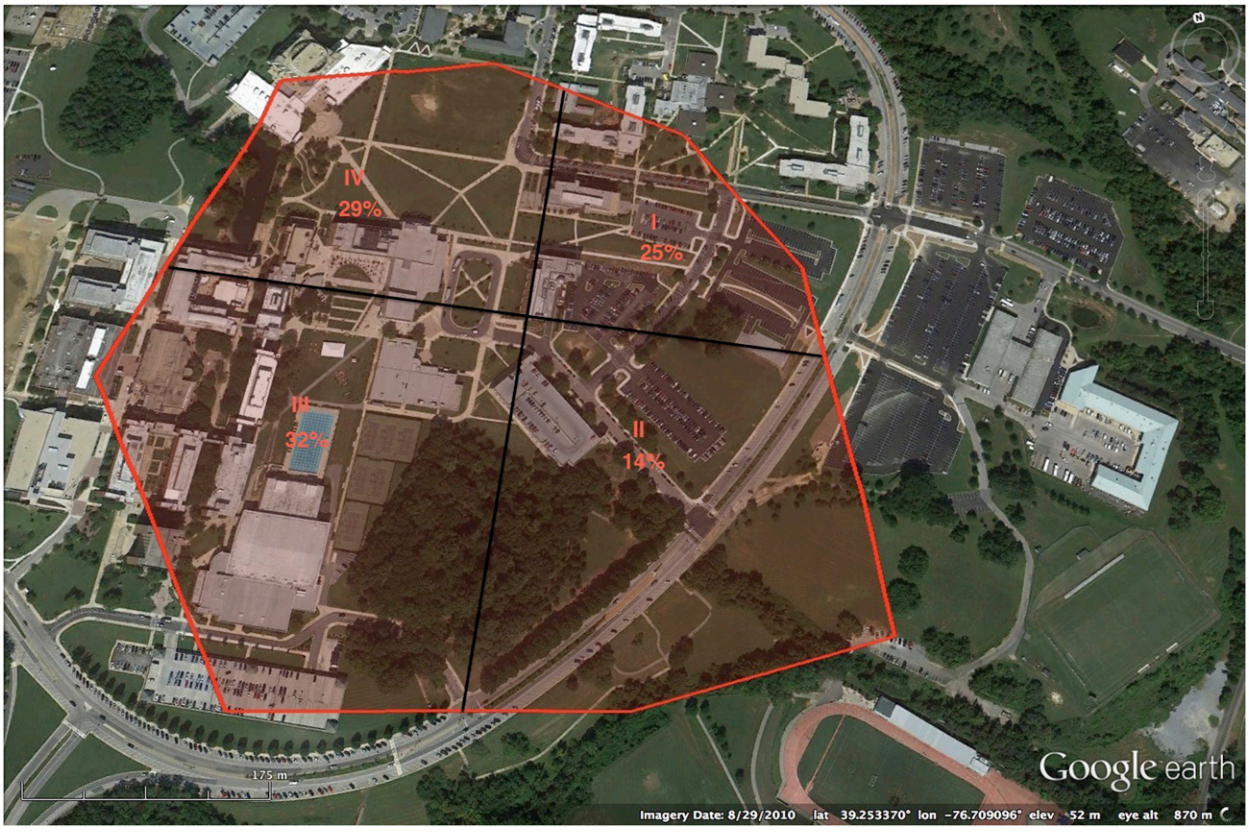

FIG. 3. Footprint of the UMBC flux tower as calculated using the Hsieh et al. (2000) model. The image is copyright Google Earth.

Broadmead and Princeton sites. For model testing, the periods for which the EC observations were missing were excluded from the modeled data (to compare averages over identical periods). To obtain a monthly average, both the model and observed flux data were separated by day and the corresponding half-hour bins from each diurnal cycle were ensemble averaged.

The modeled latent and sensible heat fluxes from all the sites are compared with their respective EC observations in Fig. 5. At the UMBC site, for which the land-cover characterization of the footprint area is very detailed, the model captures the nighttime and early-morning trends and the peak values well. In particular, the model captures the observed increase in sensible heat flux that starts around 0630–0700 eastern daylight time (EDT). During the peak hours, 1100–1300 EDT, the model slightly overpredicts both H and LE; the peak time for modeled LE is also earlier than in observations (this result might be due to inaccuracies in the thermal properties of vegetated surfaces that are used in PUCM). Given the aerodynamic and thermal heterogeneities of the urban landscape, PUCM does reasonably well in predicting the surface energy fluxes at UMBC. The root-mean-square error (RMSE, which reflects the skill of the model in reproducing accurately and precisely the modeled diurnal flux) for H is $\sim 36\ \mathrm{W\ m^{-2}}$, and the mean bias error (MBE, which represents the skill of the model in representing the fluxes averaged over the whole day) is $2.3\ \mathrm{W\ m^{-2}}$. For LE, the RMSE and MBE are 31 and $2.3\ \mathrm{W\ m^{-2}}$, respectively (note that the RMSE for LE at the UMBC site increased from 23.5 to $36\ \mathrm{W\ m^{-2}}$ from the drier first half of the month to the wetter second half). At the suburban Cub Hill site, shown in Fig. 5b, the model performs well in predicting the trends of the fluxes but the magnitude is slightly low for both H and LE. This result suggests the presence of inaccuracies in the outgoing radiation or storage terms in the model that are most likely related to inaccuracies in the surface properties and characteristics we imposed. Specifying surface properties for highly heterogeneous urban surfaces is a difficult task, particularly for a footprint as large as the Cub Hill site where the EC measurements are made at a height of 41 m AGL. The RMSEs for H and LE at Cub Hill were 54 and $53\ \mathrm{W\ m^{-2}}$, respectively. At the Princeton site, the model overpredicts both sensible and latent heat fluxes, most likely because of changes in footprint composition with wind direction that are not accounted for in our simulations. The peak time is captured well for the sensible heat

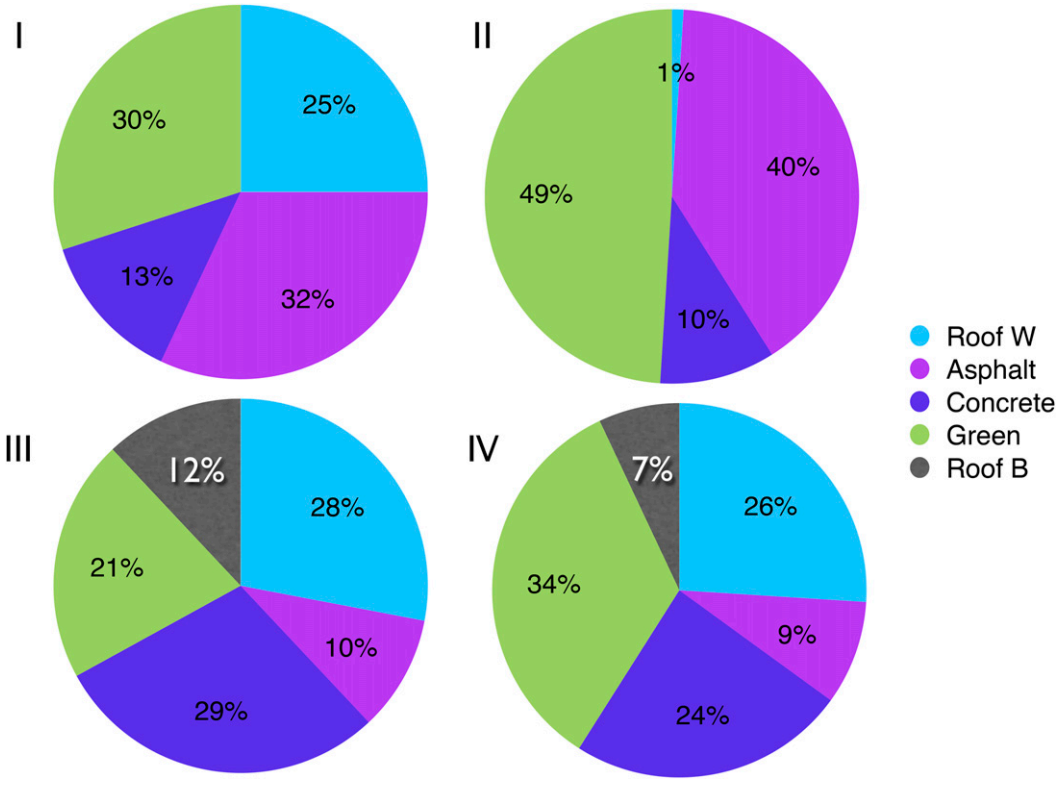

FIG. 4. Pie charts detailing the land-cover characteristics of each sector at UMBC.

flux, but modeled latent heat flux peaks earlier in the model as with the UMBC site; the site's RMSEs for H and LE were 31 and 53 W m^{-2}, respectively. At the more homogenous Broadmead site, the model performs well in predicting the latent heat flux but underpredicts the sensible heat flux. The RMSEs for H and LE at Broadmead were 34 and 36 W m^{-2}, respectively.

Although the RMSEs for H at all four sites are similar and are comparable to the performance of other UCMs (Ryu et al. 2011), the modeled LE values display more intersite variability and their RMEs range from 34 to 74 W m^{-2}. Overall, the comparisons do not reveal significant consistent bias (both fluxes are overestimated and underestimated at different sites) and confirm, despite the moderate discrepancies with observations, that PUCM is able to represent the dissimilarities between urban and suburban sites in the phases, magnitudes, and ratios of the fluxes. This result indicates that PUCM is able to capture the underlying physical processes that control the surface energy budget in built terrains with varying degrees of urbanization but that there is room for improvement, particularly in the characterization of the hygrothermal properties of the surface, in modeling the available energy. Other potential improvements consist of including in PUCM the capacity to represent tall vegetation and the deep root transpiration it induces (this work is under way), the absence of which might explain the underestimation of LE and its high RMSE at suburban sites dominated by mature tall vegetation.

3. Model results

The model results are organized into three sections that discuss the subfacet heterogeneity in terms of surface temperatures, the surface energy budget of individual subfacets, and the influence of hydrometeorological conditions on the overall SEB. The model was evaluated for all four sites, but the results section mainly focuses on the UMBC site. The focus on a detailed analysis of one site is tied to the goals of the paper, which are to link the urban SEB to the underlying materials and heterogeneity rather than to catalog and study the SEB of various sites. The UMBC site was chosen because its mix of various impervious and pervious surfaces provides a suitable platform to investigate the impact of subfacet heterogeneity and material properties; it has comparable fractions of asphalt, concrete, rooftops, and grass surfaces.

a. Surface temperature

Considerable differences in surface temperatures over various subfacets were observed at UMBC during July of 2009, as depicted in Fig. 6. While the surface temperature

Table 3. Surface and material characteristics used in PUCM; additional details about the specification and calibration of these parameters can be found in Wang et al. (2011b). Here, PR indicates Princeton, UM indicates UMBC, and CB indicates Cub Hill.

Properties	Values
Thermal roughness length for roof surface	0.001 m
Thermal roughness length for canyon-to-air exchanges	0.005 m
Momentum roughness length for roof surface	0.01 m
Momentum roughness length for canyon-to-air exchanges	0.05 m
Roof surface albedo	PR: 0.15; UM: 0.5 for white and 0.1 for black; CB: 0.3
Wall surface albedo (brick)	0.25
Ground surface albedo (asphalt; concrete; grass)	(0.15; 0.40; 0.10)
Roof surface emissivity	(0.95)
Wall surface emissivity (brick)	(0.95)
Ground surface emissivity (asphalt; concrete; grass)	(0.95; 0.95; 0.93)
Roof volumetric heat capacity	$1.8 \times 10^6\,\mathrm{J\,K^{-1}\,m^{-3}}$
Wall volumetric heat capacity (brick)	$1.2 \times 10^6\,\mathrm{J\,K^{-1}\,m^{-3}}$
Ground volumetric heat capacity (asphalt; concrete; green)	$(1.0; 2.4; 1.2) \times 10^6\,\mathrm{J\,K^{-1}\,m^{-3}}$
Roof thermal conductivity	$0.6\,\mathrm{W\,K^{-1}\,m^{-1}}$
Wall thermal conductivity	$1.3\,\mathrm{W\,K^{-1}\,m^{-1}}$
Ground thermal conductivity (asphalt; concrete; green)	$(1.2; 1.8; 1.2)\,\mathrm{W\,K^{-1}\,m^{-1}}$
Internal constant building temperature	23°C
Initial wall temperature	19°C
Initial ground surface temperature	21°C
Initial volumetric soil moisture	$0.2\,\mathrm{m^3\,m^{-3}}$
Saturated soil water content	$0.33\,\mathrm{m^3\,m^{-3}}$
Residual soil water content	$0.06\,\mathrm{m^3\,m^{-3}}$
Saturated soil hydraulic conductivity	$3.38 \times 10^{-6}\,\mathrm{m\,s^{-1}}$
Depth of water holding for ground concrete and asphalt pavements	0.001 m
Depth of water-holding capacity for roofs	
UMBC (mostly flat roofs but no gravel cover)	0.0002 m
Princeton site (many gravel roofs that do not drain well and have a high water-holding capacity)	0.002 m
Cub Hill (very flat inclined roofs)	0.0 m

over asphalt is the highest, white roofs remain the coolest. The difference in average peak surface temperature between these two surfaces is close to 15°C. In contrast to white roofs, black roofs peak at 40°C. The difference observed here is due to their respective albedos (their other thermal properties are equal). In PUCM, the white roofs were modeled with an albedo of 0.5 and the black roof's albedo was set at 0.1. Grass surfaces experience midday peak surface temperatures of ~36°C. Concrete, the third modeled impervious surface, experiences peak temperatures close to 37°C, which is significantly lower than the values for asphalt and black roofs and very comparable to that of the grass surfaces, but concrete subfacets become the hottest surfaces during the night and early-morning periods. The behavior of concrete is directly linked to its high thermal inertia or effusivity [$e = (\rho c K)^{1/2}$, where ρ is the density, c is the specific heat capacity, and K is the thermal conductivity], which allows it to store large amounts of thermal energy (due to high heat capacity) over larger depths (due to high thermal conductivity) and to release it later during the night. This results in slower diurnal variation of surface temperatures.

The differences in thermal effusivities, along with differences in the sky-view factors, also explain the differences in the timing of peak surface temperatures for the different subfacets. Because of their low thermal effusivities and their shading in the morning and afternoon, asphalt ($e = 1.2 \times 10^6\,\mathrm{J\,K^{-1}\,m^{-2}\,s^{-1/2}}$) and grass vegetated ($e = 1.44 \times 10^6\,\mathrm{J\,K^{-1}\,m^{-2}\,s^{-1/2}}$) subfacets have sharp temperature peaks that occur around 1300 EDT. Concrete, because of its high thermal effusivity ($e = 4.3 \times 10^6\,\mathrm{J\,K^{-1}\,m^{-2}\,s^{-1/2}}$), peaks around 1330 local time, with relatively slow variation around the peak. Roofs have a low thermal effusivity ($e = 1.08 \times 10^6\,\mathrm{J\,K^{-1}\,m^{-2}\,s^{-1/2}}$) that is close to that of asphalt; they hence have a peak temperature that occurs at the same time. During the cool-down periods of the afternoon, asphalt and green surfaces cool the fastest because of shading and low thermal effusivity. Roofs cool relatively slower despite their low effusivity, which is comparable to that of asphalt; this is in fact due to their higher sky-view factor in the afternoon, which results in longer exposure to solar and atmospheric radiative heating. Concrete is the slowest to cool down, despite the shading effect, because of its high thermal inertia/effusivity.

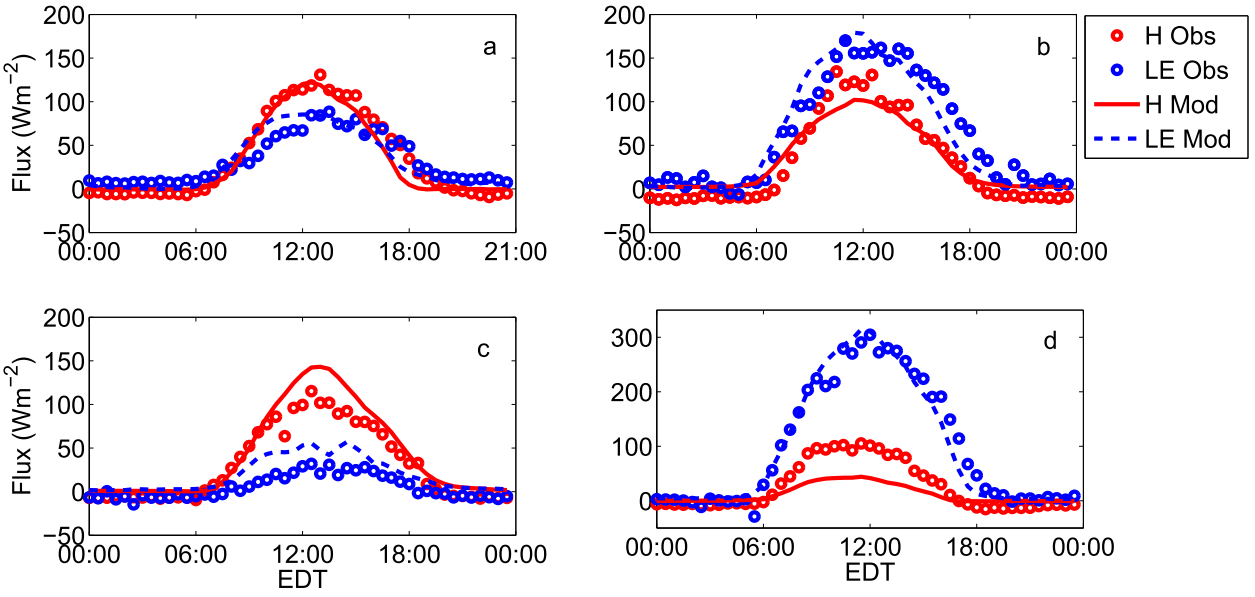

FIG. 5. Monthly-averaged diurnal cycles of surface energy fluxes H and LE with 30-min resolution, calculated by PUCM and measured using EC systems for the (a) UMBC, (b) Cub Hill, (c) Princeton, and (d) Broadmead sites, for a summer month.

These different diurnal temperature patterns of the pervious and impervious surfaces—in particular, concrete—result in the delayed peak fluxes in urban areas, as illustrated by the observational data of Fig. 2. Concrete also sustains the higher temperatures of the urban areas beyond the diurnal radiative forcing and into the nighttime. This, along with the nighttime longwave radiative trapping in the canyon that leads to all canyon facets cooling down at a slower rate than roofs (after ~2000 EDT) as depicted in Fig. 6, explains why sensible turbulent heat fluxes often continue to be positive (upward) over cities throughout the night (Lagouarde et al. 2006). This analysis reveals that concrete, despite its high albedo of 0.4, is the main material responsible for these fluxes. Asphalt, on the other hand, has a much lower albedo that allows it to have the highest daytime peak temperatures, but its low thermal effusivity does not allow it to store sufficient thermal energy to keep it hot at night. Asphalt and other material with low effusivity are only able to store energy near the surface. Another important factor that these simulations illustrate is that nighttime radiative trapping in the canyon is responsible for maintaining higher surface temperatures for canyon subfacets, relative to roofs or open vegetation.

The surface temperature trends modeled here are very close to observations made over these respective surfaces. Wang et al. (2013), for example, used IR guns to infer temperature values over multiple urban surfaces and to validate PUCM. Offerle et al. (2005) also measured

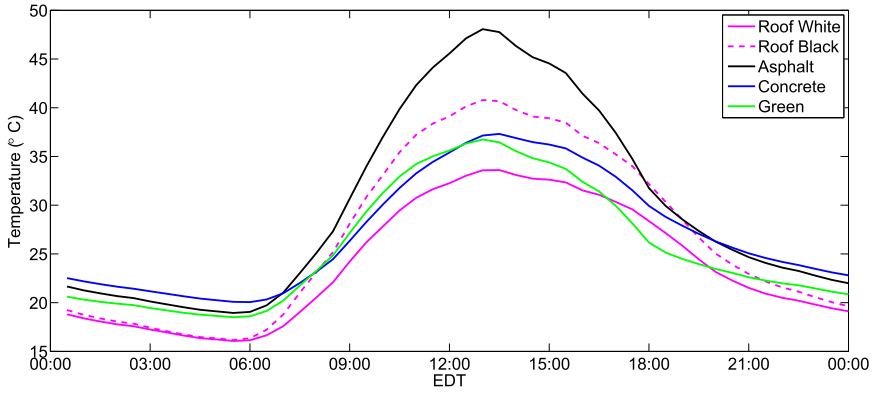

FIG. 6. Monthly-averaged diurnal cycles of subfacet temperatures at the UMBC site, with 30-min resolution, for July 2009.

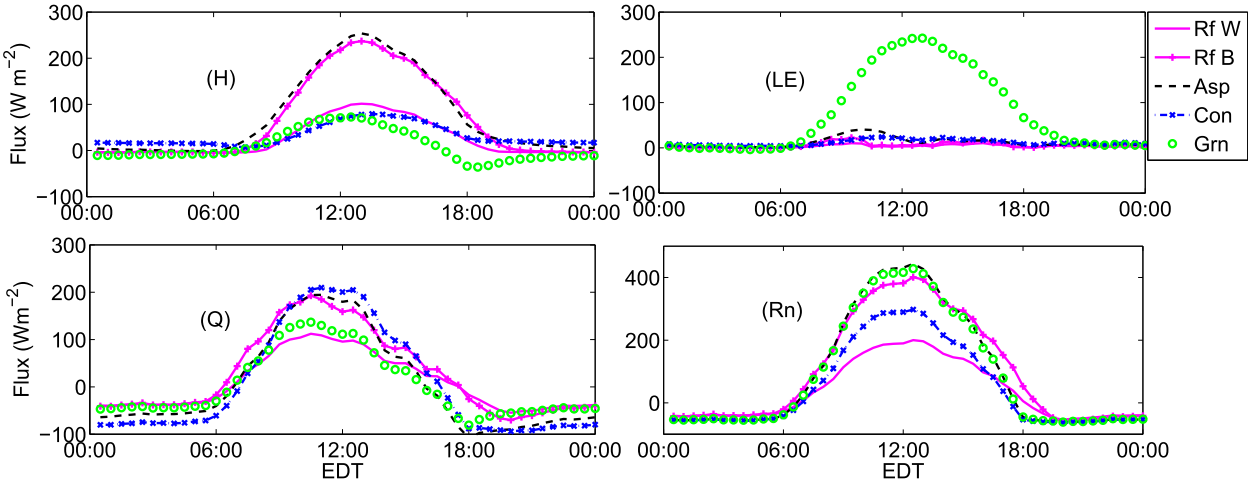

FIG. 7. Comparison of monthly-averaged diurnal cycles of (top left) sensible, (top right) latent, and (bottom left) ground heat fluxes and (bottom right) net radiation from different facets as modeled by PUCM for UMBC for July 2009.

surface temperatures that are comparable in values and trends to the ones modeled here.

b. *SEB of urban facets*

This section focuses on how the surface thermal dynamics and surface temperatures of the different materials presented in the previous section are translated into sensible and latent heat fluxes into the atmosphere and on what role they play in influencing the bulk urban surface energy budget. We first compare the different components of the SEB (H, LE, Q, and R_n) over various subfacets (Fig. 7). The reader is referred back to Table 3, which lists the thermal properties of the urban materials adopted to run the model. We reiterate that these values are selected on the basis of a thorough literature survey in addition to a calibration procedure for some of them, as detailed and validated in Wang et al. (2011a, 2013). To obtain the plots shown in Fig. 7, each sector (Fig. 4) was independently simulated by PUCM for one month (July 2009) and the fluxes from all sectors were averaged for each subfacet, weighted by the fraction covered by that subfacet type in each sector. The results hence show average fluxes for each subfacet that aggregate the simulations of all sectors (recall that for these results that do not include comparison with observations, we no longer use the wind direction to select a single sector for fluxes). The daily averages of the results in Fig. 7 give the fractional contributions of all facets to the overall energy budget terms at UMBC, which are shown in Fig. 8 along with the fraction of the surface covered by a given type of subfacet.

The rooftops, unaffected by shadowing, benefit from maximum sky-view factor at all times and thus display a marginally broader diurnal R_n cycle. The highest net radiation is, however, directly related to albedo: asphalt, grass, and black roofs display the highest peaks. This indicates that these subfacets will have the most energy that can be converted to sensible heating of the air (H) or to sensible heating of the solid ground (Q) or to latent heat (LE).

The highest sensible heat fluxes occur over asphalt subfacets (over 250 W m^{-2}), which cover 22% of the surface at UMBC (because of the large parking lots) but produce about 46% of the sensible heat fluxes (Fig. 8). Concrete surfaces contribute slightly over 20% of the total sensible heat flux and produce the highest nighttime H, with peaks around 85 W m^{-2}; this is related to their high storage of heat during daytime as detailed in the previous section. The sensible heat flux is also dominant (in comparison with latent heat flux) over both black and white roofs; peak H is ~220 W m^{-2} for black roofs, as compared with ~100 W m^{-2} for white roofs (Fig. 7). The diurnal cycles of H and Q, are broader for the black roofs relative to white roofs since they are hotter than the air or the lower ground layers for longer periods. Black roofs start releasing sensible heat 1 h earlier than white roofs and also continue emitting sensible heat for 1 h longer.

Despite their high net radiation, green surfaces produce relatively low sensible heating since a large fraction of incoming energy is diverted into latent heat. Figure 8 shows low H contribution from the grass cover; the average peak was ~80 W m^{-2}. Trees and lawns occupy nearly 33% of the area around the UMBC site (recall that both are modeled as grass-covered soils) but release 80% of the LE: the averaged midday peak was 225 W m^{-2}. The latent heat flux over impervious surfaces was intermittent; this intermittency is related to precipitation being the primary trigger for LE from these surfaces, which have

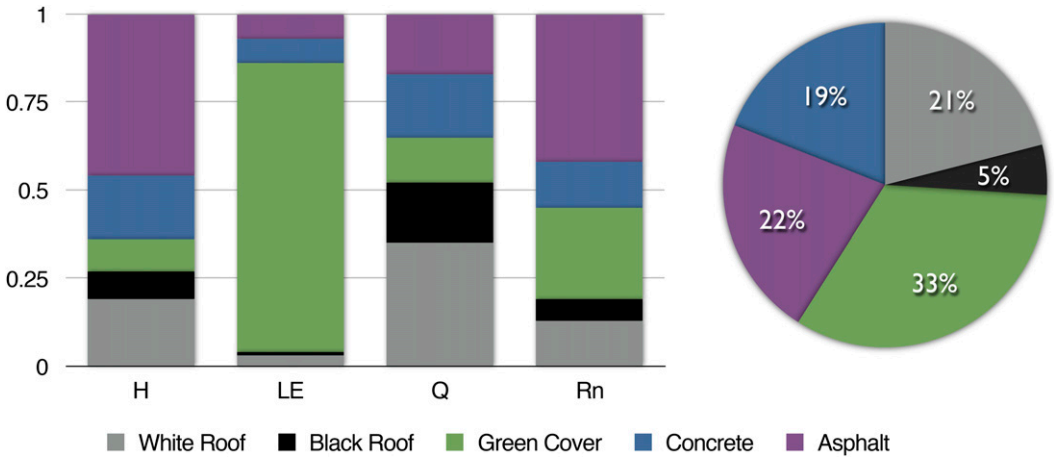

FIG. 8. (left) The bar chart details the relative contribution of each urban subfacet to the total sensible, latent and ground heat flux; these contributions include the effect of the surface fraction covered by a given subfacet. Also shown is net radiation. (right) The pie chart shows the overall land-cover distribution at the UMBC site.

very low water storage capacity. The pattern of impervious LE is thus related to the random patterns of precipitation, as well as to the diurnal SEB cycle. Concrete and asphalt surfaces contributed the most (~7% each of the total) to LE.

Concrete and asphalt produce large storage terms (Q = ground heat flux) exceeding 200 W m^{-2}; both also produce the largest negative ground fluxes during the night (sustained for longer periods for concrete), indicating that this stored energy is being released and is heating the urban air as confirmed by the positive H during nighttime for these two materials. Ground heat flux over black roofs peaks at ~160 W m^{-2}, as compared with 95 W m^{-2} over white roofs (Fig. 7). These roof fluxes are sustained in the afternoon, but they do not translate into considerable negative Q at night, probably because of low effusivity as well as the rapid radiative cooling of the roofs, which are not affected by longwave nighttime radiative trapping.

To visualize the relative importance of each individual term in the energy budget equation with respect to net radiation and to focus on the SEB of each subfacet rather than on the different components of the SEB, the monthly averaged daytime (0800–1500 local time) ratios of H/R_n, LE/R_n, and Q/R_n are plotted in Figs. 9 and 10 for all of the facets. The daytime variations (0800–1500 local time) of the energy terms over the white and black roofs when normalized by net radiation are broadly similar, but with higher storage fraction for the white roof and higher atmospheric fluxes for the black roof (Fig. 9). This result can be explained by the higher efficiency of H relative to Q: as the black roof surface gets hotter (relative to the white roof), heat convection to the atmosphere H is more efficiently performed than heat conduction to the roof Q (Bateni and Entekhabi 2012), resulting in a larger H/Q ratio for black roofs than for white roofs. The reader is reminded that Q over black roofs remains larger than Q over white roofs in absolute terms. The LE fraction of R_n is roughly constant at about 10%. As the day progresses, however, the storage flux fractions decrease and the atmospheric sensible flux fractions increase. The explanation of this change parallels the comparison between black and white roofs: the colder solid surfaces early in the morning are able to absorb a significant amount of thermal energy; as their temperatures increase, however, their ability to absorb more energy is reduced (surface gradients decrease) while the fluxes into the atmosphere are enhanced because of higher surface temperatures and the onset of convective conditions. In other words, the atmosphere is a much larger reservoir than the ground and its temperature increase per unit surface heat flux absorbed is lower, which allows it to absorb more heat.

Over asphalt (Fig. 10), the storage flux fraction is dominant between 0800 and 1100 local time but goes to almost zero or slightly negative values after 1400 local time. The contribution from LE to the overall SEB over asphalt is relatively significant early in the day but decreases also to zero around noon. This is probably due to nighttime precipitation or precipitation from the late afternoon of the previous day that results in stored water at the surface, until enough energy becomes available to evaporate it early the next morning. By noon, however, the stored water is depleted and LE drops sharply. The LE rises again later in the afternoon, probably because of afternoon rainfall. As with roofs, when the atmosphere becomes unstable and the surface heats up then

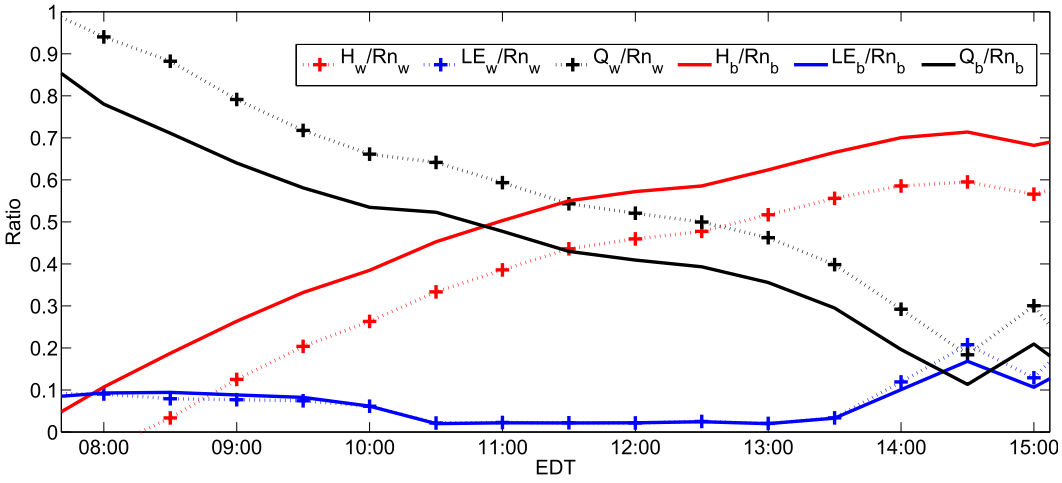

FIG. 9. Averaged contribution of sensible (H), latent (LE), and storage (Q) flux with respect to net radiation (Rn) over roof subfacets at the UMBC site. The subscripts "w" and "b" refer to white roof and black roof, respectively.

sensible heat becomes the most dominant term of the asphalt SEB.

Over concrete, because of its high effusivity, storage flux is the most dominant term almost throughout the day (except in the later afternoon). The Q/R_n ratio is consistently greater than 0.6. The H/R_n ratio over concrete increases during the afternoon as the influence of Q decreases, but it remains very low overall relative to other surfaces. As expected, the LE/R_n ratio over concrete is low, around 0.2 during the daytime period, but an increase is again observed in the afternoon because of rainfall during that period.

In contrast to impervious surfaces, LE dominates over pervious grass surfaces for most of the day. During the morning period between 0800 and 1000 EDT, however, Q is the main flux over pervious grass surfaces. The contribution of H/R_n over grass is steady at about 18% for most of the daytime. Grass surfaces are unique in that they are the only subfacet over which the LE/R_n ratio increases as the day progresses; this is related to steadiness in the surface water availability and to the complex dependence of the evaporative fraction on the diurnal cycles of the various parameters that affect it (atmospheric humidity and temperature, radiation, and soil moisture). The evaporative fraction trends for the vegetated surfaces implied by our results are in good agreement with the trends observed and theoretically derived over natural terrain (Gentine et al. 2011).

Apart from the contribution of each term to the subfacet SEB, the switchover time of which flux is dominant

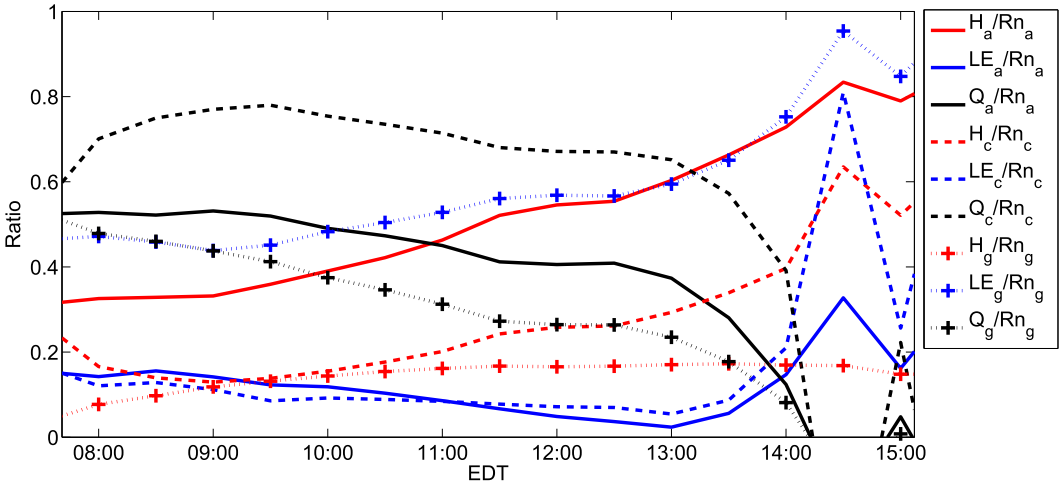

FIG. 10. As in Fig. 9, but over ground facets. The subscripts "a," "c," and "g" refer to asphalt, concrete, and grass surfaces, respectively.

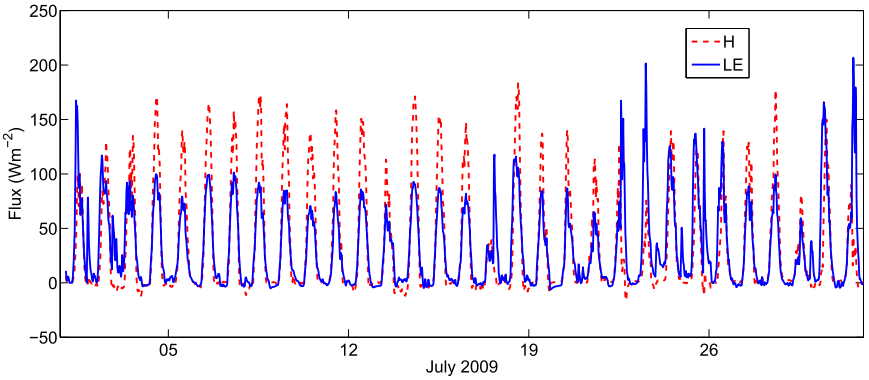

FIG. 11. The 30-min-averaged modeled latent and sensible heat fluxes for July 2009 at UMBC.

is significant to the phase lag observed between each term in the overall SEB. Over asphalt and grass surfaces, the switchover from Q to H and LE, respectively, can be related to the growth of the convective boundary layer that aids and enhances turbulent mixing. The concrete surfaces keep storing heat for most of the day; this heat is then steadily released during the evening and nighttime periods. As mentioned above, the averaged sensible heat flux over concrete never goes below zero, indicating that concrete behaves as a source of heat for the atmosphere all day long. This property of concrete to retain and release heat throughout the night is mainly responsible for nighttime UHI effects felt in large cities as explained earlier, along with the longwave canyon radiative trapping. These storage dynamics also contribute to the phase shift in peak times observed between urban, with a lot of concrete, and rural areas, with little concrete.

c. *Dry–wet contrast*

During the first half of July in 2009, the weather around the UMBC site was dry. The total precipitation for the first 15 days of the month was low in comparison with the previous 10 days. As a consequence, Bo (=H/LE) was greater than 1 and increased systematically during that dry period as shown in Fig. 11. During 1–15 July, sensible heat flux dominated latent heat flux. With increased precipitation during the relatively wet second half of the month, however, the averaged daytime Bo decreased from 1.6 to 1. Latent heat fluxes from the whole urban area peaked at over 200 W m^{-2} during the second half of July 2009 in model simulations, with a Bo of less than 0.5 on some days (e.g., the very last day plotted in Fig. 11).

To assess the effect of wetting and drying periods on the SEB of different subfacets, the budget components for a dry period (8–17 July) and a wet period (23–31 July) were plotted separately in Figs. 12 and 13, respectively. The most striking observation is the difference in LE between the wet and dry periods over the green surfaces: whereas this LE for the wet period peaks at ~280 W m^{-2}, the corresponding peak during the dry period is ~215 W m^{-2}. The evaporation from these vegetated

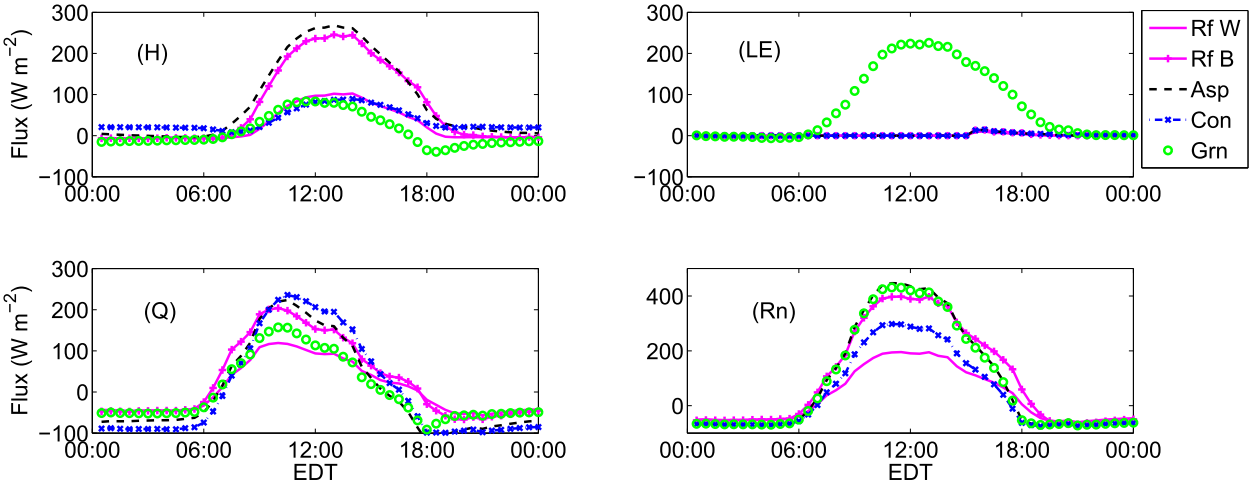

FIG. 12. Subfacet SEB for the dry period (8–17 Jul 2009) at the UMBC site.

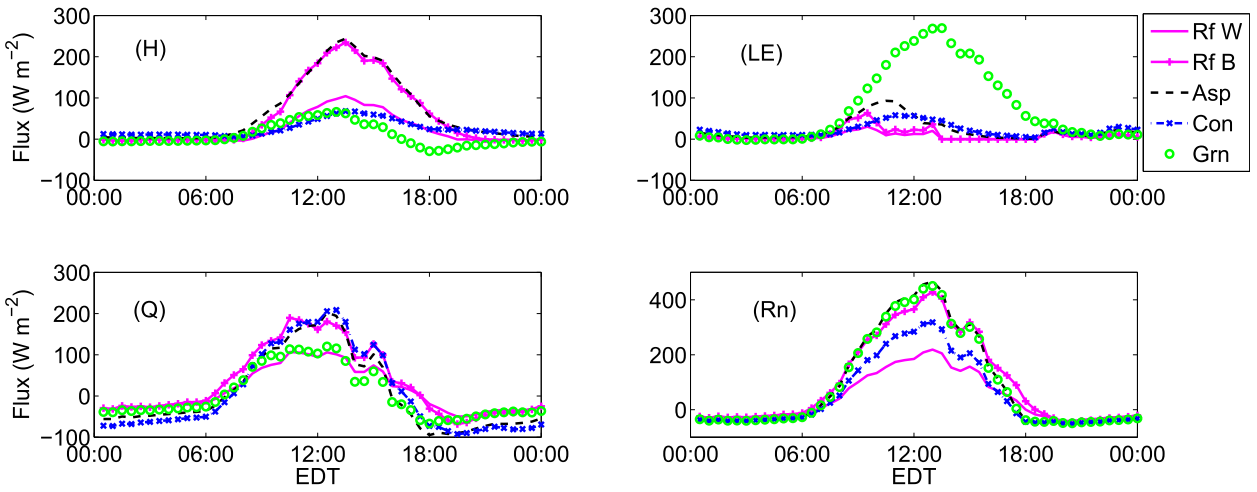

FIG. 13. As in Fig. 12, but for the wet period (23–31 Jul 2009).

surfaces is sustained into the early evening, resulting in a negative H (cooling of urban air) during both periods. Apart from the grass surfaces, the contribution from impervious surfaces to LE significantly increases during the wet period relative to the dry period. Whereas the contribution from impervious surfaces toward net LE is 7.3% for the dry period, during the wet period this contribution increased to 27% of the total (accounting for the different fractions of the area of UMBC covered by the different surfaces). On a per-unit-area basis, concrete and asphalt subfacets show peaks in LE at ~50 W m^{-2} and 80 W m^{-2}, respectively. The increased evaporation during wet periods directly affects H and Q partitioning. The peak H and Q values for the dry period over all subfacets are higher relative to those in the wet period. The peak H and Q over asphalt and concrete during the dry period were $H_{\text{asphalt}} = 268$, $Q_{\text{asphalt}} = 224$, $H_{\text{concrete}} = 87$, and $Q_{\text{concrete}} = 235$ W m^{-2}, whereas during the wet period they were reduced to 240, 190, 67, and 200 W m^{-2} respectively. The reduction in peak H from the vegetated subfacets was even more pronounced; it decreased from 95 W m^{-2} during the dry period to 60 W m^{-2} during the wet period.

These results indicate that, in addition to the differences observed between wet and dry periods in built surface evaporation, significant changes in fluxes are also expected over urban vegetated surfaces. These vegetated surfaces, when water stressed, contribute more to H. When precipitation is abundant, however, their dynamics change and contribute significantly to the cooling of urban, and suburban areas. The effect of irrigation was not accounted for in our model [and can explain some of the differences with observed data; see a discussion on urban irrigation with some results for Baltimore in Bhaskar and Welty (2012)], but our comparison of wet and dry periods implicitly indicates that if urban grass surfaces are irrigated then a significant impact on the urban SEB should be expected, in particular in suburban areas with large vegetated fractions.

4. Summary and conclusions

This study focused on understanding the influence of urban subfacet heterogeneity, and the associated influence of material properties, on the urban surface energy budget. The Princeton Urban Canopy Model was first evaluated over multiple sites and then applied over the most heterogeneous of these sites, UMBC, to simulate energy exchanges of each subfacet with the atmosphere. Our main conclusions are as follow:

- Pairs of densely built urban and suburban sites exhibit sharp contrasts in the magnitude and phase of sensible and latent heat fluxes. PUCM is able to capture these contrasts and their diurnal trends.
- Engineered surfaces, especially asphalt and black roofs, partition most of the incoming energy into sensible heat flux during the day, which results in increased air temperatures. Asphalt pavement covered 22% of the surface at UMBC but produced ~46% of the sensible heat fluxes. These dark surfaces also had the highest values of net radiation, which was mainly controlled by surface albedo.
- Concrete, while still producing more sensible than latent heat flux, partitions most of the daytime radiative energy into ground storage because of its high thermal effusivity. This high storage of thermal energy in concrete is the main agent responsible for the observed lag in peak flux times between urban and rural/suburban neighborhoods and in the sustained nighttime warming (positive H) of the urban air.

- Another important factor in the nighttime urban warming is the longwave radiative trapping in the canyons, which, as we show here, results in slower cooling of the canyon surfaces relative to the roof surfaces that have a sky-view factor of 1.
- Impervious surfaces principally partition the incoming energy into sensible heat flux and ground heat flux, but their contribution to latent heat flux cannot be ignored. At the UMBC site over the month of July 2009, nearly 17% of the observed latent heat flux was due to impervious surface evaporation, most of it following precipitation events.
- Among the impervious surfaces, concrete and asphalt contributed significantly to evaporative fluxes. Together, concrete and asphalt accounted for 14% of the overall LE at the site for the whole month.
- These characteristics of the urban SEB over different subfacets are, however, very sensitive to the availability of surface moisture and hence to precipitation. During the first, dry half of the simulated month, all surfaces produced high sensible and ground heat fluxes. During the second, wet half, in contrast, the pervious surfaces were partitioning the available energy overwhelmingly into LE, and the sensible fluxes from impervious surface were also reduced appreciably. The vegetated pervious grass surfaces that dot the urban landscape thus play a dual role: during wet periods they redistributed much of the available energy into evaporative fluxes, but when moisture stressed they behaved more like impervious built surfaces. Irrigation of these urban vegetated surfaces will thus have an important impact on surface SEB.

Overall, this study aims to stress that all ''built impervious surfaces'' are not ''engineered'' equal. There are large differences in their thermal properties and water storage abilities that, when combined with the complicated radiative processes in urban canopies, produce very heterogeneous and transient conditions. Although this can be viewed as a problem because of the complexity of the resulting dynamics, it is also potentially an asset for building designers, urban planners, and policy makers, who could exploit these differences to improve the urban environment and to make cities more resilient in the face of climate extremes, particularly heat waves. Pervious surfaces in suburbs and cities are nowadays engineered rather than ''natural'' facets, and they can also be designed with specific aims in mind.

Acknowledgments. This work was supported by NSF under CBET-1058027, CBET-1058038, and DEB-1027188; by NOAA under NA07OAR4170518; by the U.S. DOE through the EEB Hub (http://www.eebhub.org, now cbei.psu.edu) under DE-EE0004261; and by the Mid-Infrared Technology for Health and the Environment (MIRTHE) NSF center. We acknowledge the assistance of Julia Miller and Joshua Cole at UMBC/CUERE in providing the UMBC datasets.

REFERENCES

Bateni, S. M., and D. Entekhabi, 2012: Relative efficiency of land surface energy balance components. *Water Resour. Res.,* **48,** W04510, doi:10.1029/2011WR011357.

Berthier, E., S. Dupont, P. G. Mestayer, and H. Andrieu, 2006: Comparison of two evapotranspiration schemes on a suburban site. *J. Hydrol.,* **328,** 635–646.

Bhaskar, A. S., and C. Welty, 2012: Water balances along an urban-to-rural gradient of metropolitan Baltimore, 2001–2009. *Environ. Eng. Geosci.,* **18,** 37–50, doi:10.2113/gseegeosci.18.1.37.

Bohnenstengel, S. I., S. Evans, P. A. Clark, and S. E. Belcher, 2011: Simulations of the London urban heat island. *Quart. J. Roy. Meteor. Soc.,* **137,** 1625–1640, doi:10.1002/qj.855.

Ching, J., 1985: Urban-scale variations of turbulence parameters and fluxes. *Bound.-Layer Meteor.,* **33,** 335–361, doi:10.1007/BF00116683.

Christen, A., 2005: *Atmospheric Turbulence and Surface Energy Exchange in Urban Environments: Results from the Basel Urban Boundary Layer Experiment (BUBBLE).* University of Basel, 140 pp.

——, and R. Vogt, 2004: Energy and radiation balance of a central European city. *Int. J. Climatol.,* **24,** 1395–1421, doi:10.1002/joc.1074.

Coutts, A. M., J. Beringer, and N. J. Tapper, 2007: Impact of increasing urban density on local climate: Spatial and temporal variations in the surface energy balance in Melbourne, Australia. *J. Appl. Meteor. Climatol.,* **46,** 477–493, doi:10.1175/JAM2462.1.

Crawford, B., C. S. B. Grimmond, and A. Christen, 2011: Five years of carbon dioxide fluxes measurements in a highly vegetated suburban area. *Atmos. Environ.,* **45,** 896–905, doi:10.1016/j.atmosenv.2010.11.017.

Foken, T., M. Göockede, M. Mauder, L. Mahrt, B. Amiro, and W. Munger, 2005: Post-field data quality control. *Handbook of Micrometeorology,* X. Lee, W. Massman, and B. Law, Eds., Kluwer Academic, 181–208.

Gentine, P., D. Entekhabi, and J. Polcher, 2011: The diurnal behavior of evaporative fraction in the soil–vegetation–atmospheric boundary layer continuum. *J. Hydrometeor.,* **12,** 1530–1546, doi:10.1175/2011JHM1261.1.

Grimmond, C. S. B., and T. R. Oke, 1999: Heat storage in urban areas: Local-scale observations and evaluation of a simple model. *J. Appl. Meteor.,* **38,** 922–940, doi:10.1175/1520-0450(1999)038<0922:HSIUAL>2.0.CO;2.

——, and ——, 2002: Turbulent heat fluxes in urban areas: Observations and a local-scale urban meteorological parameterization scheme (LUMPS). *J. Appl. Meteor.,* **41,** 792–810, doi:10.1175/1520-0450(2002)041<0792:THFIUA>2.0.CO;2.

——, J. A. Salmond, T. R. Oke, B. Offerle, and A. Lemonsu, 2004: Flux and turbulence measurements at a densely built-up site in Marseille: Heat, mass (water and carbon dioxide), and momentum. *J. Geophys. Res.,* **109,** D24101, doi:10.1029/2004JD004936.

——, and Coauthors, 2010: The International Urban Energy Balance Models Comparison Project: First results from phase 1. *J. Appl. Meteor. Climatol.,* **49,** 1268–1292, doi:10.1175/2010JAMC2354.1.

——, and Coauthors, 2011: Initial results from phase 2 of the International Urban Energy Balance Model Comparison. *Int. J. Climatol.,* **31,** 244–272, doi:10.1002/joc.2227.

Hamdi, R., and G. Schayes, 2008: Sensitivity study of the urban heat island intensity to urban characteristics. *Int. J. Climatol.,* **28,** 973–982, doi:10.1002/joc.1598.

Hsieh, C., G. Katul, and T.-W. Chi, 2000: An approximate analytical model for footprint estimation of scalar fluxes in thermally stratified atmospheric flows. *Adv. Water Resour.,* **23,** 765–772, doi:10.1016/S0309-1708(99)00042-1.

Järvi, L., C. S. B. Grimmond, and A. Christen, 2011: The Surface Urban Energy and Water Balance Scheme (SUEWS): Evaluation in Los Angeles and Vancouver. *J. Hydrol.,* **411,** 219–237, doi:10.1016/j.jhydrol.2011.10.001.

Kusaka, H., and F. Kimura, 2004: Coupling a single-layer urban canopy model with a simple atmospheric model: Impact on urban heat island simulation for an idealized case. *J. Meteor. Soc. Japan,* **82,** 67–80, doi:10.2151/jmsj.82.67.

——, H. Kondo, Y. Kikegawa, and F. Kimura, 2001: A simple single-layer urban canopy model for atmospheric models: Comparison with multi-layer and slab models. *Bound.-Layer Meteor.,* **101,** 329–358, doi:10.1023/A:1019207923078.

——, F. Chen, M. Tewari, J. Dudhia, D. O. Gill, M. G. Duda, W. Wang, and Y. Miya, 2012: Numerical simulation of urban heat island effect by the WRF model with 4-km grid increment: An inter-comparison study between the urban canopy model and slab model. *J. Meteor. Soc. Japan,* **90B,** 33–45, doi:10.2151/jmsj.2012-B03.

Lagouarde, J.-P., M. Irvine, J.-M. Bonnefond, C. S. B. Grimmond, N. Long, T. R. Oke, J. A. Salmond, and B. Offerle, 2006: Monitoring the sensible heat flux over urban areas using large aperture scintillometry: Case study of Marseille city during the ESCOMPTE experiment. *Bound.-Layer Meteor.,* **118,** 449–476, doi:10.1007/s10546-005-9001-0.

Martilli, A., A. Clappier, and M. W. Rotach, 2002: An urban surface exchange parameterisation for mesoscale models. *Bound.-Layer Meteor.,* **104,** 261–304, doi:10.1023/A:1016099921195.

Masson, V., 2000: A physically-based scheme for the urban energy budget in atmospheric models. *Bound.-Layer Meteor.,* **94,** 357–397, doi:10.1023/A:1002463829265.

Nottrott, A., S. Onomura, A. Inagaki, M. Kanda, and J. Kleissl, 2011: Convective heat transfer on leeward building walls in an urban environment: Measurements in an outdoor scale model. *Int. J. Heat Mass Transfer,* **54,** 3128–3138, doi:10.1016/j.ijheatmasstransfer.2011.04.020.

Nunez, M., and T. Oke, 1977: Energy balance of an urban canyon. *J. Appl. Meteor.,* **16,** 11–19, doi:10.1175/1520-0450(1977)016<0011:TEBOAU>2.0.CO;2.

——, and ——, 1980: Modeling the daytime urban surface energy balance. *Geogr. Anal.,* **12,** 373–386, doi:10.1111/j.1538-4632.1980.tb00043.x.

Offerle, B., C. S. B. Grimmond, K. Fortuniak, and W. Pawlak, 2006: Intraurban differences of surface energy fluxes in a central European city. *J. Appl. Meteor. Climatol.,* **45,** 125–136, doi:10.1175/JAM2319.1.

——, ——, and ——, 2005: Heat storage and anthropogenic heat flux in relation to the energy balance of a central European city centre. *Int. J. Climatol.,* **25,** 1405–1419, doi:10.1002/joc.1198.

Oke, T. R., 1978: *Boundary Layer Climates.* Methuen, 372 pp.

——, 1988: The urban energy balance. *Prog. Phys. Geogr.,* **12,** 471–508, doi:10.1177/030913338801200401.

Porson, A., I. N. Harman, S. I. Bohnenstengel, and S. E. Belcher, 2009: How many facets are needed to represent the surface energy balance of an urban area? *Bound.-Layer Meteor.,* **132,** 107–128, doi:10.1007/s10546-009-9392-4.

Rotach, M. W., and Coauthors, 2005: BUBBLE—An urban boundary layer meteorology project. *Theor. Appl. Climatol.,* **81,** 231–261, doi:10.1007/s00704-004-0117-9.

Roth, M., 2007: Review of atmospheric turbulence over cities. *Quart. J. Roy. Meteor. Soc.,* **126,** 941–990, doi:10.1002/qj.49712656409.

Ryu, Y.-H., J.-J. Baik, and S.-H. Lee, 2011: A new single-layer urban canopy model for use in mesoscale atmospheric models. *J. Appl. Meteor. Climatol.,* **50,** 1773–1794, doi:10.1175/2011JAMC2665.1.

Song, T., and Y. Wang, 2012: Carbon dioxide fluxes from an urban area in Beijing. *Atmos. Res.,* **106,** 139–149, doi:10.1016/j.atmosres.2011.12.001.

Velasco, E., S. Pressley, R. Grivicke, E. Allwine, L. T. Molina, and B. Lamb, 2011: Energy balance in urban Mexico City: Observation and parameterization during the MILAGRO/MCMA-2006 field campaign. *Theor. Appl. Climatol.,* **103,** 501–517, doi:10.1007/s00704-010-0314-7.

Wang, Z., E. Bou-Zeid, S. K. Au, and J. A. Smith, 2011a: Analyzing the sensitivity of WRF's single-layer urban canopy model to parameter uncertainty using advanced Monte Carlo simulation. *J. Appl. Meteor. Climatol.,* **50,** 1795–1814, doi:10.1175/2011JAMC2685.1.

——, ——, and J. A. Smith, 2011b: A spatially-analytical scheme for surface temperatures and conductive heat fluxes in urban canopy models. *Bound.-Layer Meteor.,* **138,** 171–193, doi:10.1007/s10546-010-9552-6.

——, ——, and ——, 2013: A coupled energy transport and hydrological model for urban canopies evaluated using a wireless sensor network. *Quart. J. Roy. Meteor. Soc.,* **139,** 1643–1657, doi:10.1002/qj.2032.